International Symposium of Research Students on Material Science and Engineering
December 20-22, 2004, Chennai, India
Department of Metallurgical and Materials Engineering, Indian Institute of Technology Madras

ErSb/GaSb METAL/SEMICONDUCTOR NANOCOMPOSITE GROWN BY MOLECULAR BEAM EPITAXY

M.P. Hanson[1], D.C. Driscoll[1], E.R. Brown[2], and A.C. Gossard[1]
[1]*Materials Department, University of California, Santa Barbara*
[2]*ECE Department, University of California, Santa Barbara*

ABSTRACT

We demonstrate the effective use of ErSb semimetallic nanoparticles embedded within a semiconducting GaSb matrix, grown by molecular beam epitaxy, to manipulate the electronic and optical properties of the composite material for a variety of applications. The resistivity, optical absorption, and photocarrier lifetimes, are all found to be greatly influenced by the size and density of the ErSb particles. The particle size and density can be controlled by growth parameters resulting in a versatile and highly tunable composite material.

1. INTRODUCTION

Epitaxial structures containing metallic particles buried within a semiconductor matrix have been demonstrated to be effective ways of manipulating the electrical properties of the host semiconductor. Superlattices consisting of ErAs particles and GaAs spacer layers have been shown to possess higher resistivity, higher electrical breakdown fields, and much shorter carrier lifetimes than pure GaAs[1]. These properties are ideal for devices that rely on high-speed photoconductors, such as high-speed photodetectors[2] and photomixers[3]. Recently, ErAs semimetallic particles have been placed at the interface of a GaAs p-n junction and were shown to substantially enhance the tunneling current[4]. GaAs/ErAs superlattices have also been used as electrical isolation layers because of their high resistivity and ability to withstand a high electrical field[5]. A similar material that absorbs at longer wavelengths would be useful. The 0.73 eV direct band gap of the GaSb host material allows strong absorption at the wavelength of 1.55 μm. The semimetallic band structure of ErSb[6] and the small lattice mismatch of less than 0.2% with GaSb make ErSb a good choice for GaSb based metal/semiconductor composite structures. Like GaSb, ErSb has a cubic lattice, however ErSb crystallizes in the rock-salt structure rather than the zincblende structure of GaSb. Growth of epitaxial complete layers of ErSb on GaSb by molecular beam epitaxy (MBE) has previously been demonstrated[7]. In this paper we examine the growth regime prior to the formation of a complete film. In this regime the ErSb spontaneously forms nanometer-sized particles similar to ErAs on GaAs[8] and InGaAs[9]. We grow and study the properties of composite materials consisting of layers of self-assembled ErSb semimetallic particles within a GaSb matrix.

2. RESULTS AND DISCUSSION

ErSb/GaSb superlattice structures were grown by solid-source MBE in a Varian Gen II machine. Depositions of ErSb are stated in monolayers (ML) as if the ErSb had grown in

a layer-by-layer growth mode (1ML of ErSb = 3 Å of film thickness). Superlattices consisting of small depositions of ErSb separated by GaSb spacer layers were investigated with x-ray diffraction, atomic force microscopy (AFM), Hall effect, ultrafast pump-probe transmission, and infrared transmission/reflection below the band-edge of GaSb. A diagram of the sample structure is shown in the inset of Figure 1. Samples were grown on both (100)-oriented unintentionally p-type GaSb substrates and (100)-oriented semi-insulating GaAs substrates with a half micron relaxed AlSb buffer layer. Further details on the growth of these structures have previously been published[10].

Atomic force microscopy (AFM) images of the surface of the superlattices showed very little increase in roughness for ErSb depositions up to 2 ML over the reference GaSb sample. In addition, the reflective high energy electron diffraction (RHEED) pattern of the GaSb surface after the growth of the superlattice maintained the same intensity and appearance as the surface prior to the superlattice. Both of these results indicate that the addition of ErSb particles has a minimal effect on the layer-by-layer growth of the GaSb. Figure 1 shows a (002) θ-2θ x-ray diffraction pattern of a 30 period superlattice with a 2 ML ErSb 20 nm GaSb repeat unit, (2 ML 30x20 nm) grown lattice matched to a GaSb substrate with a 500 nm AlSb buffer. Superlattice peaks are clearly visible, demonstrating good coherence in the growth direction.

In addition to the superlattice samples, uncovered depositions of ErSb were grown for AFM study of ErSb particle formation. Depositions of 0.1 ML, 0.5 ML, 1 ML, and 2.5 ML of ErSb on 500 nm of GaSb were grown on relaxed 500 nm AlSb buffers nucleated on semi-insulating GaAs substrates. AFM images of these samples are shown in Figure 2. From the AFM images it is clear that the ErSb forms islands similar to those that have been observed for ErAs on both GaAs[11] and InGaAs[9,12]. It is also noted that the islands form preferentially along a $[0\bar{1}1]$ direction, which suggests that the Er adatoms migrate faster along this direction. This was also observed for ErAs grown on InGaAs[9] but not for ErAs on GaAs[8,11]. For the 0.1 ML deposition the height of the islands is between 5 Å and 9 Å and the average particle area was 70 nm^2 with a density of $1.1x10^{11}$ cm^{-2}. As the deposition is increased to 0.5 ML, the density of particles increases to about $2.2x10^{11}$ cm^{-2}, with the average particle area increasing to 120 nm^2. By increasing the deposition to 1 ML the particle density is reduced to about $1.5x10^{11}$ cm^{-2} while the average particle area increases to 300 nm^2. The height of the islands remained relatively constant between 10 Å and 16 Å (or about 4 ML) for these depositions. The particle density decreases as particles coalesce to form larger particles. This phenomenon continues in the 2.5 ML sample as the density is further reduced to $4x10^{10}$ cm^{-2} and the average particle area increases to 1300 nm^2.

To study the dependence of growth rate on ErSb particle formation three samples were grown using different ErSb growth rates but maintaining the same period and ErSb deposition. Figure 3 shows atomic force microscopy images of two samples with uncovered 0.75 ML ErSb depositions. The left image (a) shows a sample grown at a rate of 0.09 ML/s, and the right image (b) shows a sample grown at a rate of 0.04 ML/s. The faster growth rate forms a higher density of smaller particles while the slower growth rate forms a layer of larger more sparsely distributed particles.

Temperature dependent Hall measurements in the van der Pauw geometry were performed on the GaSb/ErSb superlattice samples grown on semi-insulating GaAs substrates to determine the in-plane bulk transport properties of the material. A GaSb reference sample was also grown under the same conditions with the same structure as the superlattice samples but containing no ErSb. The reference GaSb layer was measured

to be p-type with a hole concentration of $3.5x10^{16}$ cm^{-3} and mobility of 600 cm^2/Vs at room temperature. This is consistent with the unintentionally p-type behavior previously observed in GaSb which has been attributed to a defect in the GaSb crystal[13]. Figure 4(a) shows the hole concentration plotted versus 1/kT, where k is Boltzmann's constant and T is the temperature, for various depositions of ErSb in 30x20 nm superlattices. In addition, the reference GaSb sample and two uniformly Er doped GaSb samples with Er concentrations of 10^{18} cm^{-3} and 10^{19} cm^{-3} are shown. Even though the 0.1 ML 30x20nm superlattice has nearly the same average concentration of Er the two samples show a different temperature dependence of carrier concentration. The carrier concentrations vary exponentially with temperature and for the superlattice samples they are strongly dependent on particle size and density. The carrier concentration allows us to calculate the position of the Fermi level in the materials. A summary of calculated Fermi level, carrier concentration, mobility, and resistivity is shown in Table I (a).

In Figure 4(b), hole concentration vs. 1/kT is plotted for various ErSb layer spacings. The thickness of each sample was kept constant by adjusting the number of periods so that the total thickness of the GaSb region was 620 nm, effectively increasing the density of particles. In addition to the measured data, a calculation of the hole concentration in GaSb is shown. This calculation assumes that the Fermi level was pinned at the published bulk Schottky barrier height between GaSb and ErSb of 500 meV below the conduction band[7] and assumes a density of states based on the GaSb effective mass coefficients of 0.25 for the heavy hole and 0.05 for the light hole. As the layers of ErSb particles are moved closer together, the hole concentration is reduced and it approaches the calculation. Table I (b) summarizes the carrier concentration, mobility, resistivity, and Fermi level for various ErSb layer spacings. The reduction of holes with decreasing layer spacing is consistent with an increase in the overlap of the depletion regions that surround the ErSb particles.

In order to measure the photo generated carrier recombination dynamics of the material, pump-probe lifetime measurements were made at a wavelength of 1.55 μm using a commercial femtosecond Er-doped-fiber-based mode-locked laser and fiber-optic components in a transmission geometry. The change in transmission after the initial pump pulse measures the change in the population of the conduction band and therefore gives the carrier recombination rate. The laser produces a pulse train with a repetition rate of 25 MHz and an average output power of 8.6 mW. We estimate an injected carrier density of ~10^{18} cm^{-3}. The pulse train from the laser is split into pump and probe arms via a 20 dB fiber splitter. The –20 dB probe beam runs through a variable delay line with a maximum delay of 300 ps before passing into a fiber-to-free-space coupler which focuses the beam onto the sample. The pump beam passes through a "U-bench" containing a mechanical chopper before being focused onto the sample via a second fiber-to-free-space coupler. The probe beam signal is collected by an InGaAs photodetector connected to a lock-in amplifier. The rise time of the leading edge of the crosscorrelation measurement is ~300 fs, which is the temporal limit of the experiment. Lifetimes were obtained by fitting the portion of the tail between 90% and 10 % of the signal peak to an exponential expression $I_0\exp(-t/\tau)$, where τ is the photocarrier lifetime. In samples exhibiting longer tails, evidence of a secondary recombination mechanism was observed. In these cases the data is better fit with the sum of two exponentials. In these cases one lifetime τ_1 represents the fast initial decay and the other τ_2 represents the slower secondary recombination. Further details of the experimental setup have previously been published[10].

Three sets of ErSb containing samples were studied. In the first set, the period of the superlattice was kept constant at 20 nm, and the ErSb deposition per layer was changed. In this set, depositions between 0.1 ML and 2 ML per layer were examined. Figure 5 shows the normalized differential transmission on a linear scale for these samples along with the reference sample. All ErSb containing samples show a faster decay than the reference GaSb layer. As shown in the inset of Figure 5, when the deposition of ErSb per layer is increased, the photocarrier lifetime is decreased. For the 2 ML case the rise time is approximately equal to the fall time indicating a maximum upper bound on the photocarrier lifetime of ~300 fs. For samples with greater than 0.5 ML of ErSb no evidence of secondary recombination, τ_2, was observed.

In the second set of samples the ErSb deposition was kept constant at 0.1 ML and the spacing between layers was varied from 5 nm to 40 nm. The number of periods was adjusted to maintain a constant active layer thickness of 620 nm. Figure 6 shows the normalized differential transmission on a log scale for these samples along with the reference sample. These samples show evidence of a slower secondary recombination mechanism indicated by the change in slope that occurs just prior to 2 ps of delay. As the thickness between ErSb layers is decreased, both the initial decay, represented by τ_1, and the secondary decay, represented by τ_2, decrease. This trend is illustrated in Figure 7(a), which shows τ_1 and τ_2 plotted as a function of layer spacing.

In order to separate the effects due to the total amount of ErSb in the sample, the ErSb particle size, and the distance between layers of particles, three samples were grown using different ErSb growth rates but maintaining the same period and ErSb deposition of 0.5 ML. In this way the particle size is changed, but the total amount of ErSb in the layer and throughout the structure is the same. As demonstrated by the AFM images in Figure 3, a faster growth rate creates a higher density of smaller particles while a slower growth rate forms a layer of larger more sparsely distributed particles. For the same ErSb deposition and superlattice period it is observed that samples grown with lower growth rates, and therefore larger ErSb particles, have shorter lifetimes. Figure 7(b) shows a plot of lifetime vs. growth rate for a deposition of approximately 0.5 ML per layer in a 20nm period superlattice.

Table I shows a summary of the photocarrier lifetimes and transport properties. The reference sample has the highest free hole concentration and the longest lifetime, exceeding 30 ps. The actual reference sample lifetime was not extracted due to the long time scale and non-exponential nature of the decay. The addition of ErSb reduces the lifetime. As shown in Table I the lifetime depends monotonically on the ErSb deposition (a), the superlattice period (b), and the ErSb growth rate (c). The lifetime decreases for higher depositions, shorter superlattice periods, and slower growth rates. Both higher ErSb depositions and slower ErSb growth rates lead to larger ErSb particles, resulting in a consistent trend of shorter lifetimes for larger ErSb particles. The experimental data suggest that the reduction of lifetime is primarily due to trap states introduced by ErSb particles rather than the change in free hole concentration. Note the opposite trends of lifetime and free hole concentrations in Table I(a) and I(b). This is not unexpected because the optically injected carrier density (~10^{18} cm^{-3}) is significantly higher than the equilibrium hole concentration (10^{15}-10^{16} cm^{-3}).

In an effort to further investigate the composite superlattice material optical transmission measurements were made over wavelengths from 1 to 8 μm. For wavelengths between 1 and 3 μm a near-IR grating monochromator was used. Both reflection and transmission spectrums were obtained. An absorption signal was calculated by subtracting the sum of the percent reflected and percent transmitted from 100. For wavelengths between 3 and 8 μm a mid-IR Fourier-transform infrared (FTIR) spectrometer was used. Because the FTIR instrument geometry prohibited

measurement of a reflection spectrum, the transmission data was normalized to a reference structure of the same thickness and composition but containing no ErSb.

An absorption peak below the bandgap of GaSb is observed for all samples containing ErSb particles. No such peak is observed in the GaSb reference sample. We attribute the strong absorption peak to plasmon resonance on the ErSb particles within the GaSb matrix. These resonances have previously been observed in ErAs particles in GaAs[14]. The strength of this peak is proportional to the total amount of ErSb in the sample. Figure 8 shows absorption spectra for three 620 nm thick layers: a GaSb reference layer, and two ErSb/GaSb superlattices containing 0.1 ML of ErSb per layer, one with a 20 nm period and the second with a 5 nm period. The intensity of the absorption peak increases as the density of ErSb particles is increased through reduction of the spacing between ErSb layers. The peak position remains constant centered at about 2.4 μm.

As the amount of ErSb per layer is increased, in addition to the increase in attenuation, the peak position shifts from about 2.4 μm to longer wavelengths (3.8 μm). Figure 9 shows dependence of the attenuation spectrum on the ErSb deposition. While the increase in attenuation is consistent with the increase in total ErSb in the sample, the shift in peak position is likely due to a combination of both change in particle shape and size with increased deposition. Figure 10(a) shows the attenuation dependence on the total amount of ErSb in the sample while Figure 10(b) shows the peak position shift with ErSb deposition. For the superlattice containing 2 ML ErSb per 20 nm period, the strength of the effective attenuation coefficient was measured to be 1.4×10^4 cm^{-1} this is stronger than the cross gap absorption of the GaSb at 1.5 μm. Decreasing the superlattice period could further enhance the strength of this attenuation.

3. CONCLUSIONS AND SUMMARY

We have demonstrated the growth and characterization of a new composite superlattice material consisting of layers ErSb nanoparticles within a GaSb matrix. The carrier concentrations, photo carrier lifetimes, and infrared absorption of the superlattices can be correlated to the microstructure of the material. This establishes a powerful way to control the properties of semiconductors by engineering of embedded nanostructures. Through this nanostructure engineering we have been able to increase the resistance of the composite material nearly a hundred times that of a reference GaSb layer. We have demonstrated sub-picosecond photocarrier lifetimes at 1.55 μm as short as 300 fs. This is a conservative estimate since we are limited by the pulsewidth of the pump laser in our experimental setup. We have also demonstrated strong optical attenuation at wavelength below the bandgap of GaSb. These properties may be useful for a variety of applications such as electrical isolation layers, high-speed photodetectors, photomixers, and infrared optical components.

This work was supported by the Office of Naval Research. The authors would like to thank Herb Kroemer and Christoph Kadow for useful discussions.

REFERENCES

[1] C. Kadow, S. B. Fleischer, J. P. Ibbetson, J. E. Bowers, A. C. Gossard, J. W. Dong, and C. J. Palmstrom, Applied Physics Letters **75,** 3548-3550 (1999).

[2] Y. Chen, S. Williamson, T. Brock, F. W. Smith, and A. R. Calawa, Applied Physics Letters **59,** 1984-1986 (1991).

[3] E. R. Brown, F. W. Smith, and K. A. McIntosh, Journal of Applied Physics **73,** 1480-1484 (1993).

[4] P. Pohl, F. H. Renner, M. Eckardt, A. Schwanhausser, A. Friedrich, O. Yuksekdag, S. Malzer, G. H. Dohler, P. Kiesel, D. Driscoll, M. Hanson, and A. C. Gossard, Applied Physics Letters **83,** 4035-7 (2003).

[5] A. Dorn, M. Peter, S. Kicin, T. Ihn, K. Ensslin, D. Driscoll, and A. C. Gossard, Applied Physics Letters **82,** 2631-2633 (2003).

[6] Q. G. Sheng, B. R. Cooper, and S. P. Lim, Journal of Applied Physics **73,** 5409-5411 (1993).

[7] A. Guivarch, Y. Ballini, Y. Toudic, M. Minier, P. Auvray, B. Guenais, J. Caulet, B. Lemerdy, B. Lambert, and A. Regreny, Journal of Applied Physics **75,** 2876-2883 (1994).

[8] C. Kadow, J. A. Johnson, K. Kolstad, and A. C. Gossard, Journal of Vacuum Science & Technology B **21,** 29-32 (2003).

[9] D. C. Driscoll, M. Hanson, C. Kadow, and A. C. Gossard, Applied Physics Letters **78,** 1703-5 (2001).

[10] M. P. Hanson, D. C. Driscoll, C. Kadow, and A. C. Gossard, Applied Physics Letters **84,** 221-3 (2004).

[11] C. Kadow, J. A. Johnson, K. Kolstad, J. P. Ibbetson, and A. C. Gossard, Journal of Vacuum Science & Technology B **18,** 2197-2203 (2000).

[12] D. C. Driscoll, M. P. Hanson, E. Mueller, and A. C. Gossard, Journal of Crystal Growth **251,** 243-7 (2003).

[13] P. S. Dutta, H. L. Bhat, and V. Kumar, Journal of Applied Physics **81,** 5821-5870 (1997).

[14] E. R. Brown, A. Bacher, D. Driscoll, M. Hanson, C. Kadow, and A. C. Gossard, Physical Review Letters **90,** 077403-1-4 (2003).

(a)

Dep. (ML)	p (cm^{-3})	Fermi (meV)	Mobility ($cm^2/V\cdot s$)	Resistivity ($\Omega\cdot cm$)	Lifetime (ps) τ_1	τ_2
ref	3.3×10^{16}	124	577	0.34	>30	>30
2	1.8×10^{16}	139	166	2.13	0.29	--
1.5	1.5×10^{16}	145	171	2.53	0.36	--
1	1.0×10^{16}	154	191	3.24	0.40	--
0.5	3.4×10^{15}	183	205	9.23	0.48	1.58
0.25	3.1×10^{15}	185	260	7.91	0.66	2.58
0.1	3.1×10^{15}	185	297	7.05	1.12	3.44

(b)

Period (nm)	p (cm^{-3})	Fermi (meV)	Mobility ($cm^2/V\cdot s$)	Resistivity ($\Omega\cdot cm$)	Lifetime (ps) τ_1	τ_2
40	8.1×10^{15}	160	346	2.24	1.37	4.08
20	3.1×10^{15}	185	297	7.05	1.12	3.44
10	1.0×10^{15}	214	314	19.5	0.92	2.88
5	8.2×10^{14}	220	235	32.6	0.57	1.34

(c)

GR (ML/s)	p (cm^{-3})	Mobility ($cm^2/V\cdot s$)	Resistivity ($\Omega\cdot cm$)	Lifetime (ps) τ_1	τ_2
0.09	2.9×10^{15}	196	10.8	0.89	2.31
0.056	2.8×10^{15}	236	9.40	0.79	2.32
0.04	3.7×10^{15}	222	7.63	0.75	2.18

Table I. Room temperature electrical properties and photocarrier lifetimes for various (a) ErSb depositions (Dep.) in a 30 period, 20nm spacing, ErSb/GaSb superlattice, (b) period spacings in a in a 620nm thick ErSb/GaSb superlattice containing 0.1 ML of ErSb per layer, and (c) ErSb growth rates for a ~0.5 ML deposition of ErSb in a 30 period, 20nm spacing, ErSb/GaSb superlattice.

FIGURES

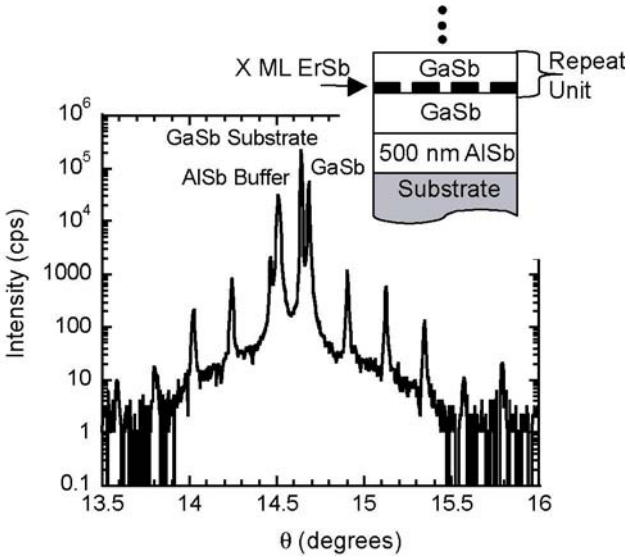

Figure 1 θ-2θ x-ray diffraction pattern of a 30x20nm GaSb 2ML ErSb superlattice grown on a GaSb substrate. The inset shows the ErSb/GaSb superlattice structure.

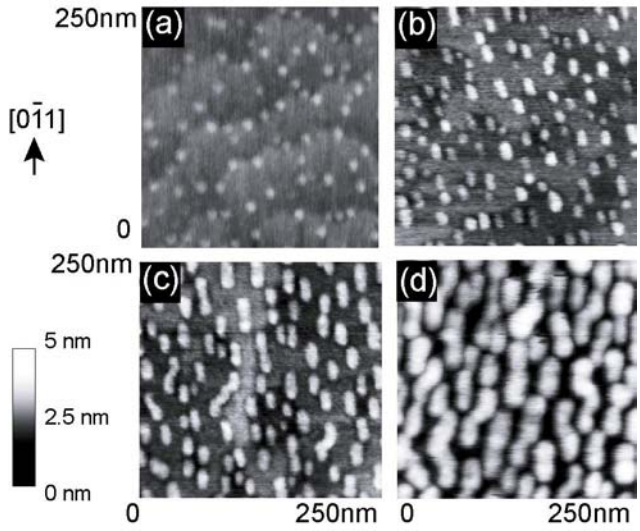

Figure 2 AFM images of ErSb particles on a GaSb surface for **(a)** 0.1 ML of ErSb, **(b)** 0.5 ML of ErSb, **(c)** 1 ML of ErSb, **(d)** 2.5 ML of ErSb. ErSb particles preferentially elongate along the [0$\bar{1}$1] direction.

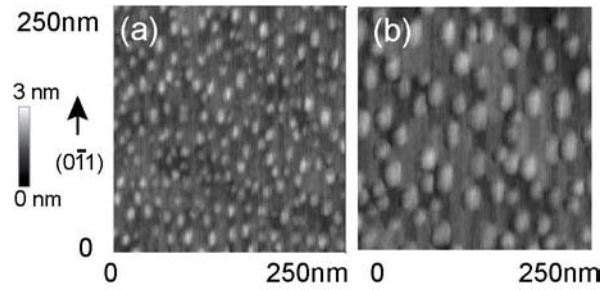

Figure 3 Atomic force microscopy image of a 0.75 ML deposition of uncovered ErSb islands on a GaSb surface grown at **(a)** 0.09 ML/s and **(b)** 0.04 ML/s.

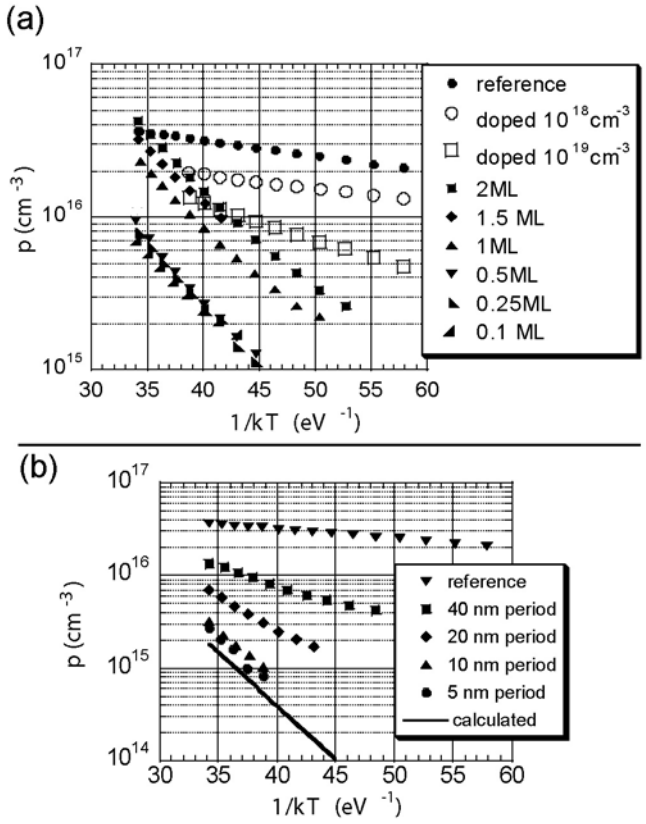

Figure 4 The hole concentration in GaSb/ErSb superlattices vs. 1/kT for **(a)** various ErSb depositions (in ML) in a 30x20nm GaSb/ErSb superlattice as well as a GaSb reference sample and two bulk Er doped GaSb films and **(b)** various *period lengths* for GaSb/0.1 ML ErSb superlattices. The total thickness of the film was kept to 620 nm by adjusting the number of periods. The calculated line shows the calculated temperature dependence of the hole concentration if the Fermi level were uniformly pinned at the published Schottky barrier height of 500 meV below the conduction band [10].

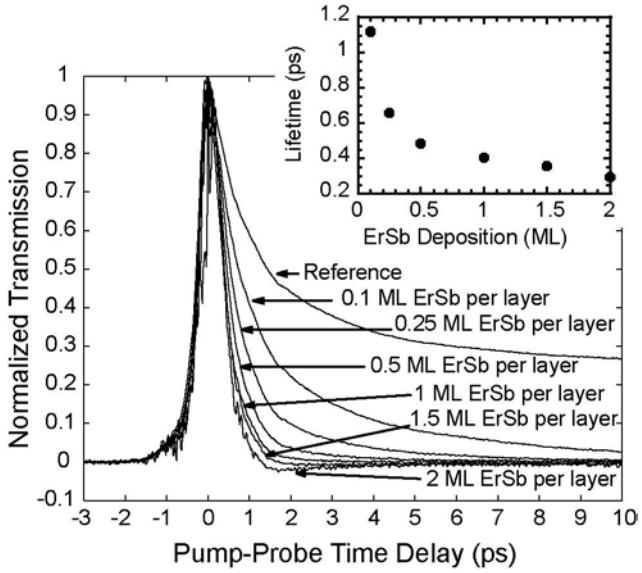

Figure 5 Normalized differential transmission ΔT/T plotted against pump-probe delay for various ErSb depositions in a 30 period, 20nm spacing, ErSb/GaSb superlattice. The inset shows the calculated lifetime τ_1 (ps) is plotted against ErSb deposition per layer in a 30 period, 20nm spacing, ErSb/GaSb superlattice.

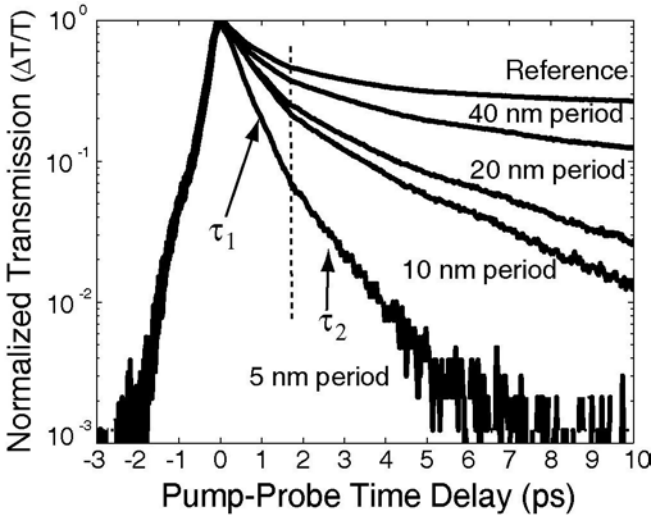

Figure 6 Normalized differential transmission ΔT/T plotted against pump-probe delay on a log scale for various layer spacings in a 620nm thick ErSb/GaSb superlattice containing 0.1 ML of ErSb per layer. The number of periods was adjusted to maintain a constant thickness thereby increasing the 3D density of ErSb particles. The section of the plot fitted to obtain τ_1 is approximately on the left side of the dashed line, while the portion fitted to obtain τ_2 is on the right.

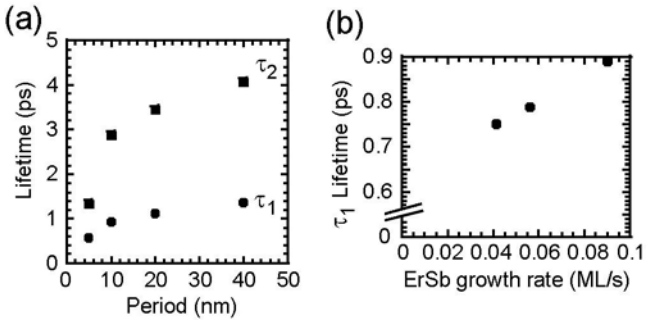

Figure 7 (a) The calculated lifetimes, τ_1 and τ_2, are plotted against period spacing in a 620nm thick ErSb/GaSb superlattice containing 0.1 ML of ErSb per layer. **(b)** The calculated lifetime τ_1 (ps) is plotted against ErSb growth rate for ~0.5 ML ErSb deposition per layer in a 30 period, 20nm spacing, ErSb/GaSb superlattice.

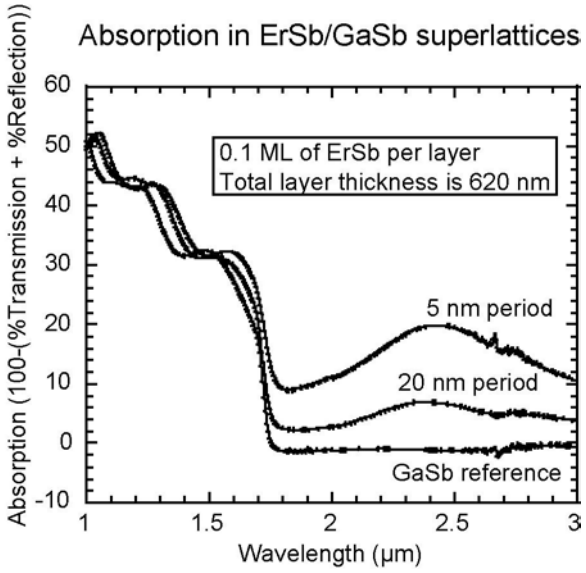

Figure 8 Dependence of sub-bandgap absorption on period (5 nm and 20 nm), in 620 nm thick ErSb/GaSb superlattices containing 0.1 ML of ErSb per layer relative to a reference GaSb layer.

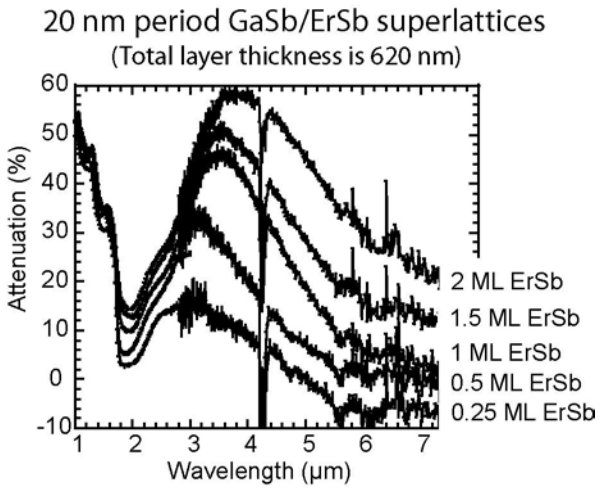

Figure 9 Attenuation of the transmission signal for various deposition of ErSb. Data from 1 to 3 μm is taken with a grating spectrometer, data from 3 to 7 μm is taken with a FTIR spectrometer.

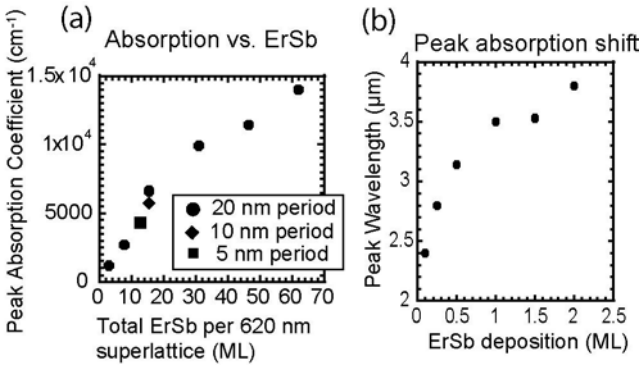

Figure 10 (a) Peak absorption plotted against the total amount of ErSb in the sample. **(b)** Peak absorption position plotted against ErSb deposition per superlattice period.